

## Surface atomic rearrangements and crystalline transformations in amorphous $\text{Fe}_{81}\text{B}_{13.5}\text{Si}_{3.5}\text{C}_2$ ribbons

N. Saegusa and A. H. Morrish

*Department of Physics, University of Manitoba, Winnipeg, Manitoba R3T 2N2, Canada*

(Received 22 April 1982)

Atomic rearrangements and crystallization within 100 nm of the surface in isochronally annealed amorphous  $\text{Fe}_{81}\text{B}_{13.5}\text{Si}_{3.5}\text{C}_2$  (METGLAS<sup>®</sup> 2605SC) ribbons have been investigated by conversion-electron Mössbauer spectroscopy. The atomic rearrangements at the dull surface, at the shiny surface, and in the bulk of the ribbon are all different. The onset of crystallization at the two surfaces occurs at lower temperatures than for the bulk. In the amorphous state, the average atomic compositions are suggested to be different in the shiny-surface layer, in the dull-surface layer, and in the bulk. The crystallization was found to consist of three steps. In the first step precipitations of Fe-(~2.0–3.0) at. % Si and Fe-(~2.5–3.5) at. % Si take place at the shiny and the dull surfaces, respectively, and in the second step crystallization of  $\text{Fe}_3\text{C}$  occurs. The process is completed by crystallization of  $\text{Fe}_2\text{B}$  and a decrease of about 1% in the silicon concentration of the Fe-Si alloys.

### I. INTRODUCTION

Amorphous-alloy ribbons produced by the planar-flow cast method using a single quenching wheel<sup>1</sup> have two distinctive surfaces. The surface in contact with the quenching wheel appears dull and opaque, whereas the other one, free of any contact, has a shiny appearance. It has been reported that the physical and chemical properties of the two surfaces and the bulk portion of the ribbon differ. For example, the atomic compositions at the surfaces of the as-quenched amorphous alloys are not the same as the nominal value.<sup>2–6</sup> Also, the onset of crystallization in isochronally annealed ribbons is different for the surfaces and the bulk.<sup>7</sup> A study that delineates the characteristics of the three portions of the ribbon, namely the shiny and the dull surface-layers and the bulk region, would be of current interest.

Transmission Mössbauer spectroscopy (TMS) has been widely employed to investigate the magnetic and crystallization properties of Fe-containing amorphous alloys. The information obtained is an average over the ribbon thickness; in other words, essentially the physical and chemical properties of the bulk portion are determined. Another approach is to detect the electrons generated by the deexcitation of those nuclei that have absorbed incident  $\gamma$  rays resonantly.<sup>8</sup> For the 14.4-keV transition of  $^{57}\text{Fe}$ , the main process of importance is the emission of *K*-shell conversion electrons that have an energy of 7.3 keV. Since these low-energy electrons have a

relatively small penetrating power, they must originate close to the surface if they are to emerge and be detected. Consequently, conversion-electron Mössbauer spectroscopy (CEMS) provides information that is an average over a surface layer about 100 nm in depth. For ribbons about 30  $\mu\text{m}$  thick, TMS and CEMS provide techniques for differentiating bulk and surface-layer properties.

In our laboratory an investigation of the surface layers of amorphous  $\text{Fe}_{81}\text{B}_{13.5}\text{Si}_{3.5}\text{C}_2$  ribbons (METGLAS<sup>®</sup> 2605SC) has been made employing  $^{57}\text{Fe}$  conversion-electron Mössbauer spectroscopy. To facilitate comparison with the bulk properties, spectra were obtained for the same as-quenched and isochronally-annealed samples used in earlier TMS experiments.<sup>9</sup>

### II. EXPERIMENTAL

Amorphous  $\text{Fe}_{81}\text{B}_{13.5}\text{Si}_{3.5}\text{C}_2$  (METGLAS<sup>®</sup> 2605SC) in a continuous ribbon form of 25.4 mm wide and about 30  $\mu\text{m}$  thick was obtained from the Allied Corporation (USA). Ribbons about 8 mm in length were placed between two stainless-steel plates about 1 mm apart; the dull side of the ribbon rested on the bottom plate. The samples were isochronally annealed in a helium-gas atmosphere slowly flowing through a conventional tube furnace; the time period was arbitrarily chosen to be 20 min. The manufacturer states that the gas is 99.995 wt. % pure He with a maximum  $\text{O}_2$  impurity of 10 ppm.

Conversion-electron Mössbauer spectra were recorded at room temperature with a continuous He—4 mol % CH<sub>4</sub> gas flow-type proportional counter, similar to that described by Swanson and Spijkerman,<sup>8</sup> and a conventional constant-acceleration Mössbauer spectrometer. The  $\gamma$ -ray source was <sup>57</sup>Co in a Rh matrix, and an  $\alpha$ -Fe foil was used for calibration.

Least-squares fitting to the spectra was made with quasi-Lorentzian line shapes<sup>10</sup> for the pattern of the amorphous phase and with Lorentzian line shapes for the patterns of the crystalline phases. The constraints applied were (1)  $A_1=A_6$ ,  $A_2=A_5$ , and  $A_3=A_4$ , where  $A_i$  is the area of the  $i$ th line of the six-line magnetic pattern, (2) for the crystalline patterns only,  $\Gamma_1=\Gamma_6$ ,  $\Gamma_2=\Gamma_5$ , and  $\Gamma_3=\Gamma_4$ , where  $\Gamma_i$  is the linewidth of the  $i$ th line, and (3) also for the crystalline patterns only,

$$\Gamma_1:\Gamma_2:\Gamma_3::1:0.92:0.89,$$

the values observed for the  $\alpha$ -Fe calibration spectrum.

It should be noted that the operating conditions for the electron counter, such as gas-flow rate, counter bias, source-sample geometry, and surface area of the sample, are not the same for each spectrum. Therefore it was not possible to obtain information on the recoilless fraction by comparing the absorption areas of the various spectra.

### III. RESULTS AND DISCUSSION

Typical CEMS spectra, all recorded at room temperature, for the shiny and dull surfaces of samples annealed at various temperatures,  $T_A$ , are shown in Figs. 1(a) and 1(b), respectively. All spectra were recorded at room temperature; for comparison purposes the spectra for the two surfaces of the as-quenched sample are also displayed. The solid lines drawn in Fig. 1 were obtained by least-squares computer fitting. For convenience of discussion, the results are categorized into three groups that depend on the surface condition of the sample: (A) the completely crystallized state, (B) coexistence of the amorphous and crystalline phases, and (C) the amorphous-only state.

#### A. Completely crystallized state ( $T_A \geq 760$ K)

CEMS spectra of the two ribbon surfaces for  $T_A \geq 760$  K were fitted with four six-line patterns;

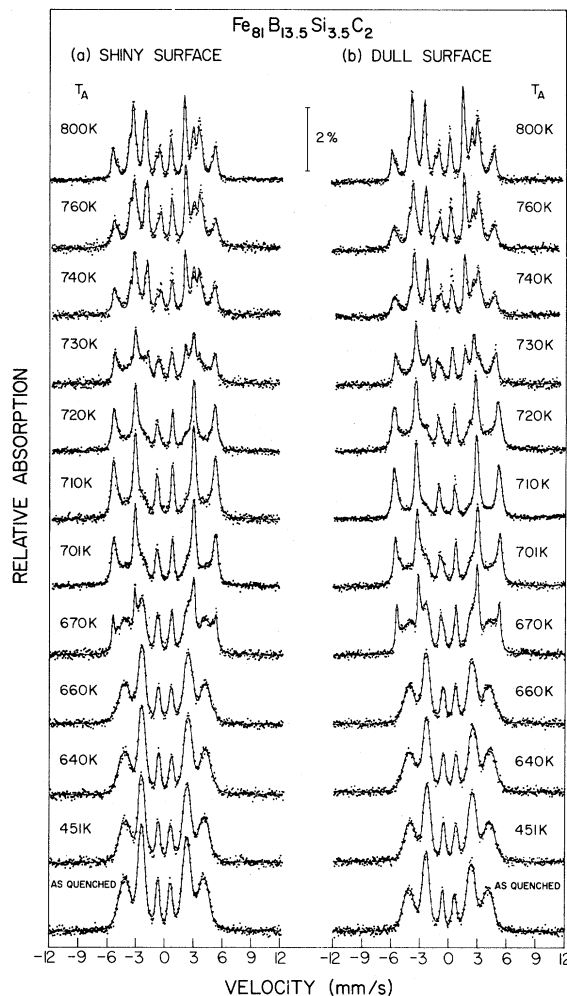


FIG. 1. Conversion-electron Mössbauer spectra at room temperature of (a) shiny and (b) dull surfaces after annealing at various temperatures  $T_A$  for 20 min. The spectra of an as-quenched sample are also displayed at the bottom of the figure.

Lorentzian line shapes, applicable for completely crystallized components, were used. The hyperfine parameters obtained are listed in Table I. Possible crystalline compounds and alloys that may be produced from amorphous Fe-B-Si-C have been listed earlier<sup>9</sup>; those that appear to correspond best with the data in Table I are listed in Table II.<sup>11-13</sup> Two patterns are for Fe-Si alloys, the third is for Fe<sub>2</sub>B, and the fourth for Fe<sub>3</sub>C.

The Si concentration of the Fe-Si alloys may be estimated from the area ratio of patterns associated with an Fe ion at sites with different numbers of Fe nearest neighbors (NN), as in the earlier TMS study.<sup>9</sup> The area ratio for eight Fe NN and seven

TABLE I. Hyperfine parameters and relative areas for patterns of four crystalline components at the surfaces of amorphous  $\text{Fe}_{81}\text{B}_{13.5}\text{Si}_{3.5}\text{C}_2$  after annealing at various temperatures  $T_A$  for 20 min.

Parameter	$T_A$ (K)	Pattern 1	Pattern 2	Pattern 3	Pattern 4
Shiny surface					
$H_{\text{hf}}$ (T)	800	33.08	30.45	23.02	21.14
$\delta$ (mm/s)		0.01	0.04	0.15	0.19
Relative area (%)		35.9	5.6	26.3	32.4
$H_{\text{hf}}$ (T)	760	32.66	29.86	23.02	20.97
$\delta$ (mm/s)		0.02	0.03	0.14	0.20
Relative area (%)		42.6	3.7	32.6	21.1
Dull surface					
$H_{\text{hf}}$ (T)	800	33.08	30.61	23.00	21.01
$\delta$ (mm/s)		0.01	0.01	0.13	0.19
Relative area (%)		30.3	9.5	32.5	27.8
$H_{\text{hf}}$ (T)	760	32.81	30.61	23.02	20.96
$\delta$ (mm/s)		0.01	0.02	0.11	0.19
Relative area (%)		38.7	6.5	26.4	28.4

Fe NN sites, calculated assuming that Si atoms are randomly distributed over the bcc lattice sites, are listed in Table III. Comparison with the data of Table I shows that the area ratio corresponding to 1 and 2 at. % Si for the shiny and dull surfaces, respectively, fit best when  $T_A = 760$  K. The change in the area ratio for eight and seven Fe NN for  $T_A = 800$  K is consistent with an ordering of the Fe-Si alloys, as observed previously by TMS for the bulk portion of the ribbon.<sup>9</sup>

The relative areas of the surface crystalline products are appreciably different from those for the bulk portion of the ribbon.<sup>9</sup> A considerable amount of  $\text{Fe}_3\text{C}$  is identified at both surfaces, whereas in the TMS experiments none was detected until a large magnetic field was applied that then resolved the small  $\text{Fe}_3\text{C}$  absorption pattern.

The atomic compositions in the surface layers about 100 nm thick may be estimated from relative area data, assuming that the recoilless fractions of the crystalline components are the same at room temperature. Table IV lists the compositions determined for  $T_A = 760$  and 800 K, the average of the two, as well as the composition for the bulk.<sup>9</sup> At both surface layers the concentration of carbon is larger, of silicon is smaller, and of boron is slightly smaller, as compared to the bulk.

It should be noted that the atomic compositions reflect those for the crystallized state, and are not necessarily the same as those for as-quenched amorphous samples since atomic diffusion to and from the surface layers may take place during the annealing. Only limited data concerning the atomic diffusion for B, Si, and C have been reported. For

TABLE II. Data on stable crystalline materials. The isomer shifts  $\delta$  are relative to  $\alpha$ -Fe foil.

Crystalline material	Structure	Site	$H_{\text{hf}}$ (T)	$\delta$ (mm/s)	Ref.
Fe-0.85 at. % Si	bcc	8 Fe NN	33.07	0.002	11
		7 Fe NN	30.97	0.037	
Fe-3 at. % Si (500 °C)	bcc	8 Fe NN	33.22	0.005	11
		7 Fe NN	30.71	0.046	
$\text{Fe}_2\text{B}$	tetragonal		23.7	0.12	12
$\text{Fe}_3\text{C}$	orthorhombic		20.8	0.29	13

TABLE III. Occupation probabilities for a random distribution of silicon in Fe-Si alloys. Here  $c$  is the Si concentration (%) and  $l$  is the number of Fe NN to a certain iron atom.

$c$ (%)	$l$	8	7	6
1		92	8	0
2		85	14	1
3		78	19	3
4		72	24	4
5		66	28	6

some amorphous alloys containing larger amounts of carbon, electron-beam heating produced little change in the carbon concentrations in the outermost 10-nm layers, even after crystallization.<sup>3</sup> However, the silicon concentration in one of the alloys did increase slightly.<sup>3</sup> In addition, in two other investigations, depletion of boron near the surface was observed in several as-quenched amorphous ribbons.<sup>5,6</sup> In summary, these results suggest that, near the surface of an as-quenched ribbon, the C concentration is larger and the Si concentration is smaller than at the interior.

#### B. Coexistence of amorphous and crystalline phases ( $660 \leq T_A \leq 740$ K)

The CEMS spectra of the shiny and the dull surfaces for  $660 \leq T_A \leq 740$  K were fitted with one set of six quasi-Lorentzian lines and one or more sets of six Lorentzian lines. Consequently, the surface layers are considered to be partially crystallized in this annealing-temperature region. The hyperfine fields and relative areas of the component patterns at the shiny and the dull surfaces are shown as a function of the annealing temperature in Figs. 2 and 3, respectively. As may be seen from Figs. 2 and 3, the onset of crystallization is first observed at

$T_A = 660$  K; then only one crystalline pattern is required. For  $T_A \geq 670$  K two crystalline patterns are required and are assigned to the Fe-Si alloy with eight Fe NN and seven Fe NN, respectively. The area ratios of the eight Fe NN and seven Fe NN patterns indicate that the Si concentrations at the shiny and the dull surfaces are  $\sim 2.5-3.5$  at. % and  $\sim 2.0-3.0$  at. %, respectively; these values are slightly larger than those for the completely crystallized state. By contrast, in the bulk portion of the ribbon, the Si concentration of the Fe-Si alloy during the early stages of crystallization is smaller than that of the completely crystallized samples.

In order to investigate the onset of surface crystallization further, surface layers about 400 nm thick were removed from the sample annealed at 670 K by polishing softly with a finger tip using 0.5- $\mu$ m alumina powder soaked in alcohol; the spectra then observed are shown in Fig. 4. By comparing the corresponding spectra in Fig. 1, it is evident that the crystalline patterns were now absent. Hence crystallization is limited to a depth at the surface of 400 nm or less. Furthermore, this experiment confirms that the onset of crystallization is nonuniform over the ribbon thickness and takes place near the surfaces at a lower annealing temperature than in the bulk.

As is evident in Fig. 3, the change in the relative areas with respect to the annealing temperature slows down at  $T_A \approx 680$  or 690 K. A similar behavior was observed at about 20°C above the temperature at which crystallization was first detected in the bulk.<sup>9</sup> This plateau was attributed to the formation of a more stable amorphous phase with the atomic composition  $\text{Fe}_{75}(\text{metalloid})_{25}$ . Although the changes in the recoilless fractions of the amorphous and crystalline components at the surface were not determined, it seems reasonable to suppose that the quasistable amorphous state found at the surface is similar to that in the bulk.

The relative areas in Fig. 3 have anomalous values at  $T_A = 710$  K, particularly for the dull sur-

TABLE IV. Estimated atomic compositions of the amorphous phase based on the relative-area data listed in Table I. The recoilless fractions of the crystalline components are assumed to be the same. The probable error in each of the atomic compositions is 1.6%.

$T_A$ (K)	Shiny side	Dull side	Bulk portion
760	$\text{Fe}_{80.8}\text{B}_{13.2}\text{Si}_{0.4}\text{C}_{5.7}$	$\text{Fe}_{81.2}\text{B}_{10.7}\text{Si}_{0.4}\text{C}_{7.7}$	
800	$\text{Fe}_{80.3}\text{B}_{10.6}\text{Si}_{0.4}\text{C}_{8.7}$	$\text{Fe}_{79.2}\text{B}_{12.9}\text{Si}_{0.3}\text{C}_{7.4}$	
760-800			
average	$\text{Fe}_{80.6}\text{B}_{11.9}\text{Si}_{0.4}\text{C}_{7.2}$	$\text{Fe}_{80.3}\text{B}_{11.8}\text{Si}_{0.4}\text{C}_{7.5}$	$\text{Fe}_{79.1}\text{B}_{15.0}\text{Si}_{3.1}\text{C}_{2.8}$ <sup>a</sup>

<sup>a</sup>Reference 9.

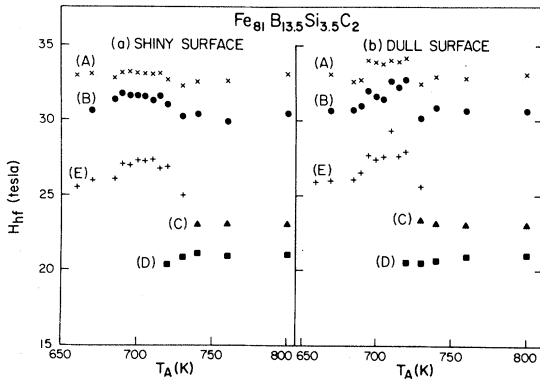


FIG. 2. Hyperfine-field dependence on annealing temperature of each component pattern above  $T_A \geq 660$  K for (a) shiny and (b) dull surfaces. Here (A) and (B) are for crystalline Fe-Si with eight Fe NN and seven Fe NN, respectively, (C) is for crystalline  $\text{Fe}_2\text{B}$ , (D) for crystalline  $\text{Fe}_3\text{C}$ , and (E) for the amorphous component. The probable errors at each point were smaller than the size of the drawn symbols.

face. This behavior may be related to the onset of crystallization of the second crystalline component,  $\text{Fe}_3\text{C}$ , at  $T_A = 720$  K. A possible interpretation is that the recoilless fraction of the amorphous component decreases as the result of unstable atomic bonding created by the incipient clustering of atoms just before the formation of  $\text{Fe}_3\text{C}$ .

At  $T_A \approx 730$  K and above the third crystalline

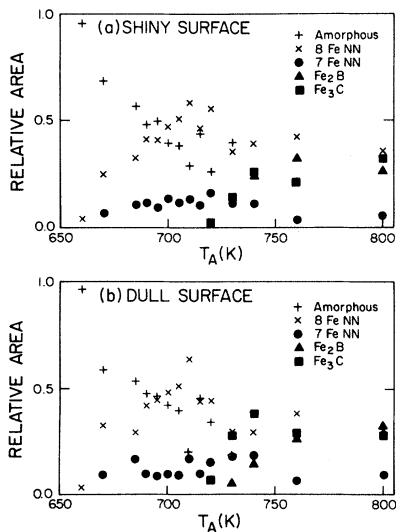


FIG. 3. Annealing temperature dependences of relative areas of each component patterns (a) of shiny and (b) of dull surfaces for  $T_A \geq 660$  K, determined from room-temperature CEMS spectra. The probable errors do not exceed the size of the data symbols.

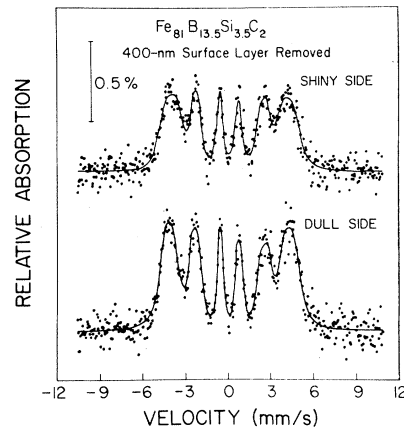


FIG. 4. CEMS spectra at room temperature (a) of the shiny-surface side and (b) of the dull-surface side for the sample annealed at 670 K after removing about a 400-nm layer from each side.

component,  $\text{Fe}_2\text{B}$ , appears; hence its influence should be considered. However, the accurate determination of the area of the amorphous pattern then becomes extremely difficult, since this area is small, the linewidths are broad, and the overlap with the crystalline patterns is large. Therefore, no further discussion is given.

The third crystalline component,  $\text{Fe}_2\text{B}$ , appears at different temperatures at the shiny and the dull surface layers, viz.,  $T_A = 740$  and  $730$  K, respectively. Because the resolution is poor, the CEMS spectra for  $T_A = 740$  K may be fitted equally well either with four crystalline patterns or with four crystalline and one amorphous patterns. The hyperfine parameters of the amorphous pattern varied depending on the initial trial values used in the computer program. Therefore, the curve displayed in Fig. 1 for  $T_A = 740$  K is that for the sum of the four crystalline patterns only.

However, the change in the relative areas with  $T_A$ , particularly for  $\text{Fe}_2\text{B}$  (Fig. 3) indicates that crystallization has not been completed at  $T_A = 740$  K. Instead, the completion of crystallization at both the shiny and the dull surfaces seems to occur at  $T_A \approx 760$  K.

As shown in Fig. 2, the hyperfine fields for crystalline Fe-Si at the dull surface become rather large for  $695 \leq T_A \leq 720$  K. The origin of these anomalies is not known. The possibility is unlikely that, in this annealing-temperature region only, the crystallization component is not an Fe-Si alloy. Perhaps the overlapping of the eight Fe NN, seven Fe NN, and amorphous patterns has introduced a systematic error.

### C. The amorphous-only state

Each spectrum for  $T_A \leq 640$  K was fitted with six quasi-Lorentzian lines. The hyperfine fields, isomer shifts, and average linewidths for the shiny and dull surfaces are shown as a function of the annealing temperature in Figs. 5(a) and 5(b), respectively. Not shown are the quadrupole shifts, which are zero within the experimental error; the same result had been observed for the bulk.<sup>9</sup> The isomer shifts are almost independent of  $T_A$ , and are about the same at both surfaces. These isomer-shift data are thus less informative than those for the bulk region.

The hyperfine fields and average linewidths of Fig. 5 indicate generally that the atomic rearrangements at the surfaces are similar to those in the bulk except that they occur at a lower temperature. Although the errors are too large to permit any definitive conclusion, the average linewidth for the shiny surface seems to decrease up to about  $T_A = 550$  K; for the bulk it decreased up to  $T_A \approx 600$  K. This reduction in the hyperfine-field distribution therefore again suggests that the short-range order has gradually increased. Also, the local maximum in  $H_{\text{hf}}$  at  $T_A \approx 550$  K for the shiny surface is observed at  $T_A \approx 600$  K in the bulk.<sup>9</sup> On the other hand, the decrease in  $H_{\text{hf}}$  up to  $T_A \approx 400$  K, especially pronounced for the dull surface, was not observed for the bulk. This change in the hyperfine fields at low annealing temperature seems to imply

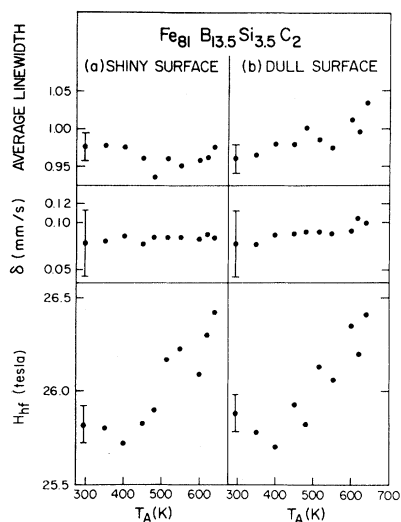


FIG. 5. Annealing temperature dependences of the hyperfine field  $H_{\text{hf}}$  (T), isomer shift  $\delta$  (mm/s), and average linewidth (mm/s) (a) for the shiny and (b) for the dull surface for  $T_A \leq 640$  K. Data for the as-quenched sample are also plotted.

that some atomic rearrangements have very small activation energies indeed.

Differences between the shiny and dull surfaces would be expected to be related, at least in part, to the different quenching rates during the production of the ribbon. Since the dull side is in direct contact with the wheel, the quenching rate is fastest, and presumably the disorder is greatest, at this surface. Unfortunately, the small differences in Fig. 5 combined with the experimental uncertainties do not permit definitive conclusions to be drawn.

### D. Surface crystallization temperature

By increasing the speed of the quenching wheel, Gránásy *et al.*<sup>14</sup> quenched an amorphous Fe-B alloy at a faster rate; they found that the ribbon bulk then had a higher crystallization temperature. Since the quenching rate is presumably fastest at the dull surface, it is reasonable to suppose that the onset of surface crystallization would occur at a temperature higher than that for the bulk. Just the opposite is observed; for  $\text{Fe}_{81}\text{B}_{13.5}\text{Si}_{3.5}\text{C}_2$  crystallization of the surface layers starts at  $T_A \approx 660$  K, whereas that of the bulk begins at  $T_A \approx 690$  K.<sup>9</sup> Therefore, the origin of the differences in the temperatures for the onset of crystallization must be sought elsewhere than in the quenching rates. The compositional differences of Table IV are suggestive and will now be considered further.

The physical properties, including the crystallization temperature, of quaternary amorphous Fe-B-Si-C alloys appears to be an average of the properties of the amorphous ternary Fe-B-Si and Fe-B-C alloys.<sup>15</sup> The crystallization temperatures of these ternary alloys are a function of their atomic compositions.<sup>16-20</sup> For  $\text{Fe}_{80}(\text{B,C})_{20}$ , one investigation reported a monotonic decrease in crystallization temperature with carbon concentration,<sup>17</sup> whereas in another a maximum in the crystallization temperature was observed for a carbon concentration of about 3 at.%.<sup>18</sup> For amorphous Fe-B-Si alloys, the crystallization temperature was found to decrease for smaller silicon concentrations.<sup>18-20</sup> Since, from Table IV, the concentration of the carbon is higher, and that of the silicon is lower in the surface layers as compared to the bulk, a lower crystallization temperature at the surface is expected on purely compositional grounds. Of course, the quenching rate may still be responsible for the compositional differences. Furthermore, other factors, including lateral diffusion, which could be faster at the surface than in the bulk, may also be operating.

## IV. CONCLUSIONS

The transformations that occur in the surface layers about 100 nm thick after amorphous  $\text{Fe}_{81}\text{B}_{13.5}\text{Si}_{3.5}\text{C}_2$  ribbons are annealed isochronally have been studied by  $^{57}\text{Fe}$  conversion-electron Mössbauer spectroscopy. Before any crystallization is detected, atomic rearrangements take place, which differ somewhat at the dull and at the shiny surfaces. Crystallization, when it does begin, is not uniform over the ribbon thickness, but instead commences at or near the outer surfaces. The crystallization was found to develop in three stages. Firstly, an Fe-Si alloy starts to precipitate at  $T_A = 660$  K, and then, secondly, crystalline  $\text{Fe}_3\text{C}$  appears at  $T_A = 720$  K. Thirdly, and finally, crystalline  $\text{Fe}_2\text{B}$  is formed at  $T_A = 740$  and  $730$  K at the

shiny and dull surfaces, respectively. The silicon concentrations of the Fe-Si alloy for the completely crystallized surface layers are 1 and 2 at. % at the shiny and dull surfaces, respectively; in the early stages of crystallization, the silicon concentrations are somewhat larger. Differences in the composition of the amorphous alloy at the surfaces compared to the bulk are suggested as one of the main reasons why crystallization in the ribbon first commences at the surfaces.

## ACKNOWLEDGMENT

This research was supported by a grant from the Natural Sciences and Engineering Research Council of Canada.

- 
- <sup>1</sup>L. A. Davis, N. DeCristofaro, and C. H. Smith, in *Proceedings of the Conference on Metallic Glasses: Science and Technology*, edited by C. Hargitai, I. Bakonyi, and T. Kemény (Central Research Institute of Physics, Budapest, 1981), Vol. 1, p. 1.
- <sup>2</sup>J. L. Walter, F. Bacon, and F. E. Luborsky, *Mater. Sci. Eng.* **24**, 239 (1976).
- <sup>3</sup>H. G. Suzuki and K. Yamamoto, *Mater. Sci. Eng.* **33**, 57 (1978).
- <sup>4</sup>D. R. Baer, L. R. Pederson, and M. T. Thomas, *Mater. Sci. Eng.* **48**, 283 (1981).
- <sup>5</sup>I. Nagy, T. Tarnóczy, M. Hossó, and F. Pavlyák, in *Proceedings of the Conference on Metallic Glasses: Science and Technology*, Ref. 1, p. 223.
- <sup>6</sup>A. Z. Nagy, B. Vasvári, P. Duwez, L. Bakos, J. Bogács, and V. M. Nazarov, *Phys. Status Solidi A* **61**, 689 (1980).
- <sup>7</sup>H. N. Ok and A. H. Morrish, *Phys. Rev. B* **23**, 2253 (1981); *J. Phys. F* **11**, 1495 (1981); *J. Appl. Phys.* **52**, 1835 (1981); P. J. Schurer, A. H. Morrish, and M. J. Stavn, *Phys. Status Solidi A* **64**, 343 (1981).
- <sup>8</sup>K. R. Swanson and J. J. Spijkerman, *J. Appl. Phys.* **41**, 3155 (1970).
- <sup>9</sup>N. Saegusa and A. H. Morrish, *Phys. Rev. B* **26**, 305 (1982).
- <sup>10</sup>D. C. Price, S. J. Campbell, and P. J. Back, *J. Phys. (Paris)* **41**, C1-263 (1980).
- <sup>11</sup>L. Häggström, L. Grånäs, R. Wäppling, and S. Devanarayanan, *Phys. Scr.* **7**, 125 (1973).
- <sup>12</sup>L. Takács, M. C. Cadeville, and I. Vincze, *J. Phys. F* **5**, 800 (1975).
- <sup>13</sup>H. Bernas, I. A. Campbell, and R. Fruchart, *J. Phys. Chem. Solids* **28**, 17 (1967).
- <sup>14</sup>L. Gránásy, A. Lovas, and T. Kemény, in *Proceedings of the Conference on Metallic Glasses: Science and Technology*, Ref. 1, p. 197.
- <sup>15</sup>F. E. Luborsky and J. L. Walter, *IEEE Trans. Magn.* **16**, 572 (1980).
- <sup>16</sup>F. E. Luborsky, J. J. Becker, J. L. Walter, and D. L. Martin, *IEEE Trans. Magn.* **16**, 521 (1980).
- <sup>17</sup>K. Shinomura, P. H. Shingu, and R. Ozaki, *J. Mater. Sci.* **15**, 1175 (1980).
- <sup>18</sup>M. Naka and T. Masumoto, *Sci. Rep. Res. Inst. Tohoku Univ. Ser A* **27**, 118 (1979).
- <sup>19</sup>K. Narita, J. Yamasaki, and H. Fukunaga, *IEEE Trans. Magn.* **13**, 1544 (1977).
- <sup>20</sup>F. E. Luborsky, J. J. Becker, J. L. Walter, and H. H. Lieberman, *IEEE Trans. Magn.* **15**, 1146 (1979).